Journal of Physics:
Condensed Matter

PAPER

Comparing LDA-1/2, HSE03, HSE06 and G_0W_0 approaches for band gap calculations of alloys

To cite this article: R R Pela *et al* 2015 *J. Phys.: Condens. Matter* **27** 505502

IOP Publishing Journal of Physics: Condensed Matter

J. Phys.: Condens. Matter **27** (2015) 505502 (10pp) doi:10.1088/0953-8984/27/50/505502

Comparing LDA-1/2, HSE03, HSE06 and G_0W_0 approaches for band gap calculations of alloys

R R Pela[1,2], M Marques[1] and L K Teles[1]

[1] Grupo de Materiais Semicondutores e Nanotecnologia, Departamento de Física, Instituto Tecnológico de Aeronáutica, 12228-900 São José dos Campos, SP, Brazil

E-mail: rrpela@ita.br

Received 21 July 2015, revised 16 October 2015
Accepted for publication 3 November 2015
Published 26 November 2015

Abstract

It has long been known that the local density approximation and the generalized gradient approximation do not furnish reliable band gaps, and one needs to go beyond these approximations to reliably describe these properties. Among alternatives are the use of hybrid functionals (HSE03 and HSE06 being popular), the GW approximation or the recently proposed LDA-1/2 method. In this work, we compare rigorously the performance of these four methods in describing the band gaps of alloys, employing the generalized quasi-chemical approach to treat the disorder of the alloy and to obtain judiciously the band gap for the entire compositional range. Zincblende InGaAs and InGaN were chosen as prototypes due to their importance in optoelectronic applications. The comparison between these four approaches was guided both by the agreement between the predicted band gap and the experimental one, and by the demanded computational effort (time and memory). We observed that the HSE06 method provided the most accurate results (in comparison with experiments), whereas, surprisingly, the LDA-1/2 method gave the best compromise between accuracy and computational resources. Due to its low computational cost and good accuracy, we decided to double the supercell used to describe the alloys, and employing LDA-1/2 we observed that the bowing parameter changed remarkably, only agreeing with the measured one for the larger supercell, where LDA-1/2 plays an important role.

Keywords: band gap, *ab initio* calculations, density functional theory, hybrid functionals, GW method, LDA-1/2

(Some figures may appear in colour only in the online journal)

1. Introduction and theoretical background

Ab initio calculations often utilize density functional theory (DFT) within the local density approximation (LDA), or the generalized gradient approximation (GGA), to predict many properties in materials research [1]. However, while LDA and GGA accurately predict many ground state properties, their eigenvalue spectra is not supposed to yield band gaps (BGs) in connection to the experimental ones—in fact, BGs calculated through GGA or LDA are significantly underestimated [2]. In some extreme cases, such as InN and InAs, materials can be mispredicted as semimetals instead of semiconductors [3].

On the other hand, many-body perturbation theory can lead to a quasi-particle (QP) band-structure in direct connection with photo-emission and photo-absorption experiments. The QP energies e_n^{QP} are the solution of

$$\left(-\frac{\nabla^2}{2}+V_H+V_n\right)\psi_n(\vec{r})+\int d^3r'\Sigma(\vec{r},\vec{r}',e_n^{QP})\psi_n(\vec{r}')=e_n^{QP}\psi_n(\vec{r}), \quad (1)$$

in which V_H and V_n are, respectively, the Hartree and the nuclei potentials. The self-energy operator Σ, within the *GW*

[2] Present address: Physics Department and IRIS Adlershof, Humboldt-Universität zu Berlin, Zum Großen Windkanal 6, D-12489 Berlin, Germany

approximation [4], is the first order term of an expansion in Feynman diagrams with respect to the screened Coulomb interaction [5]:

$$\Sigma(\vec{r},\vec{r}',\omega) = \frac{\mathrm{i}}{2\pi}\int \mathrm{d}\omega' \mathrm{e}^{\mathrm{i}\eta\omega'} G(\vec{r},\vec{r}',\omega+\omega')W(\vec{r},\vec{r}',\omega'), \quad (2)$$

in which G is the single-particle Green's function, W the dynamically screened Coulomb interaction, and η a infinitesimally small number. In principle, the equations that appear in the *GW* method must be solved self-consistently, because both G and W depend on the solutions of equation (1). In practice, this is mostly avoided by employing DFT (or another starting point) wavefunctions and eigenvalues as input for the calculation of the first order correction, in a method known as G_0W_0 [6, 7], which gives the QPs eigenvalues as

$$e_{\mathrm{n}}^{\mathrm{QP}} = e_{\mathrm{n}}^{\mathrm{KS}} + Z_{\mathrm{n}}\langle\psi_n|\mathrm{Re}[\Sigma^{G_0W_0}(e_{\mathrm{n}}^{\mathrm{KS}})] - V_{\mathrm{XC}}|\psi_n\rangle, \quad (3)$$

in which V_{XC} is the exchange and correlation potential, and $Z_{\mathrm{n}} = (1-\partial\Sigma/\partial e)^{-1}$ is the renormalization factor. Although G_0W_0 is only a single-shot correction, and sometimes may depend critically on the starting point (wavefunctions from DFT, hybrid functionals, or other choices [6–10]), it has yielded good results for BGs, direct and inverse photoemission spectra, alignment of energy levels, quantum transport in nanoscale junctions, core-level spectroscopy, pump–probe spectroscopy, and so on. However, the microscopic dielectric function, necessary to evaluate W, is very costly to calculate, and its calculation is responsible for making *GW* a very computationally involved approach [5].

An alternative approach, less costly than G_0W_0 but more accurate than LDA and GGA, are the hybrid functionals, in which one mixes a certain amount of Hartree–Fock exchange interaction with GGA. In this case, most of the computational difficulties arise from the evaluation of the slowly decaying Fock exchange $E_{\mathrm{X}}^{\mathrm{HF}}$ (also called exact exchange) with distance [6]. In consideration of this problem, Heyd *et al* proposed a more tractable hybrid-functional scheme for extended systems [6, 11], giving rise to the Heyd–Scuseria–Ernzerhof (HSE) functional. The proposal is to substitute the exchange energy in the conventional GGA Perdew–Burke–Ernzerhof (PBE) [12] functional by a functional which mixes Hartree–Fock exchange energy and PBE, only for a certain range

$$E_{\mathrm{X}}^{\mathrm{HSE}} = \alpha E_{\mathrm{X}}^{\mathrm{HF,SR}}(\mu) + (1-\alpha)E_{\mathrm{X}}^{\mathrm{PBE,SR}}(\mu) + E_{\mathrm{X}}^{\mathrm{PBE,LR}}(\mu). \quad (4)$$

Here, α defines a mixing parameter (usually taken as $\alpha = 0.25$) between the short-range Hartree–Fock exchange energy $E_{\mathrm{X}}^{\mathrm{HF,SR}}(\mu)$ and the short-range PBE energy $E_{\mathrm{X}}^{\mathrm{PBE,SR}}(\mu)$; μ is the parameter which determines the screening, defining the range of the Hartree–Fock correction [6]. This is handled by decomposing the Coulomb kernel into a short-range and a long-range term [7], according to

$$\frac{1}{r} = \frac{\mathrm{erfc}(\mu r)}{r} + \frac{\mathrm{erf}(\mu r)}{r}, \quad (5)$$

in which erf and erfc are, respectively, the error and the complementary error function. Choosing $\mu = 0.3\,\text{Å}^{-1}$ leads to the HSE03 functional, whereas $\mu = 0.2\,\text{Å}^{-1}$ leads to the HSE06 functional. The long-range exchange energy is given only by the PBE term, and the correlation energy comes entirely from PBE. In general, the use of HSE-type hybrid functionals has shown significant improvements in the description of BGs [7, 13–15], band offsets [6, 7, 16], and defect levels [17–19], and the prediction of accurate direct–indirect BG crossovers [16]. Nevertheless the gain of accuracy increases the computational cost by one or two orders of magnitude compared to conventional (semi)local DFT [5, 7].

In this sense, the recently proposed LDA-1/2 is an appealing method for BG calculations [20–22]. It approximately remedies the absence of derivative discontinuity of LDA and approximately includes the self-energies of QPs (these two issues are the main causes for the LDA and other (semi)local failures in predicting well the BGs [23]), and hence provides good descriptions for BGs of binary semiconductors [20, 21] and alloys [2], for localized states in magnetic semiconductors [24, 25], for band-offsets of interfaces [26–28], and also for defect-formation energies in semiconductors [29, 30]. The advantages of this method are (i) its low computational cost, comparable to a traditional LDA (or GGA) calculation, (ii) its simple implementation, making the method easily applicable within several *ab initio* approaches, such as pseudopotential calculations, the projector augmented wave (PAW), and the linearized augmented plane wave (LAPW), and (iii) it is free of empirically adjusted/adjustable parameters. The LDA-1/2 method recalls the Slater transition state technique [31], and it is based on Janak's theorem [32] and on the assumption of a linear behavior of eigenvalues with the occupation of KS orbitals [21, 33]. The ionization energy of a certain Kohn–Sham (KS) orbital is, thus, equal to its eigenvalue calculated with half occupancy. When applied to semiconductors, for which the BG depends on the ionization energy I and the electron affinity A, this half-occupation scheme turns out to furnish the BG E_{g} as

$$E_{\mathrm{g}} = I - A = e_{\mathrm{cond}}(1/2) - e_{\mathrm{val}}(1/2), \quad (6)$$

where e denotes one KS eigenvalue and the subscripts refer to the top of the valence band (val) or to the bottom of the conduction band (cond). Instead of calculating crystals with half-occupied KS orbitals, fortunately, it is possible to subtract from the KS potential V_{KS} the so-called 'self-energy potential' $V_{\mathrm{S}}(\vec{r})$, and perform a normal full-occupation calculation, but with eigenvalues that correspond to those with half-ionized orbitals. The modified KS equation then reads

$$\left[-\frac{\nabla^2}{2} + V_{\mathrm{KS}}(\vec{r}) - V_{\mathrm{S}}(\vec{r})\right]\psi_i(\vec{r}) = e_i\psi_i(\vec{r}), \quad (7)$$

where i spans the desired number of bands. V_{S} is obtained from an atomic calculation, as the difference between KS potentials of the half-ionized and the normal atom [20, 22]. This potential V_{S} is to be calculated for each atom in the crystal, and, in order to avoid numerical issues caused by the 'tail' $1/(2r)$ of the Coulomb potential, it must be trimmed with the aid of a cutting function

$$\Theta(r) = \left[1 - \left(\frac{r}{\mathrm{CUT}}\right)^8\right]^3. \quad (8)$$

The parameter CUT is determined variationally by making the BG extreme [20, 21], so that the method still remains fully *ab initio*.

In this work, we compare the performance of the four aforementioned methods in describing the BG of alloys, a task which is more challenging than the calculation for isolated compounds. Zincblende $In_xGa_{1-x}As$ and $In_xGa_{1-x}N$ were chosen as benchmarks because In-based III–V compounds have unique optical and electronic properties, being often used in lasers, light-emitting diodes and detectors for optical communication, instrumentation and sensing [34–36]—therefore, an accurate prediction of the electronic properties of InGaAs and InGaN alloys is important. Apart from the technological importance, InAs and InN also pose a challenging work, because they are mispredicted by LDA and GGA as semimetals rather than semiconductors. To rigorously describe these alloys, we employ a statistical approach, the generalized quasi-chemical approximation (GQCA), to obtain the BG as a continuous function of x. The alloy is regarded as an ensemble of statistically independent clusters, and the BG of each cluster is calculated with the LDA-1/2, HSE03, HSE06 and G_0W_0 methods.

2. Methodology to study the alloys

The calculations were performed with the Vienna *Ab-initio* Simulation Package (VASP), employing the projector augmented wave (PAW) method [37, 38]. The In 4d and Ga 3d levels were treated as valence band levels. For InGaAs, a cutoff energy for plane waves of 340 eV was used; for InGaN, 400 eV. Initially, we employed a cubic supercell containing eight atoms (four cations and four anions—see figure 1), similar to the one used by Teles *et al* in [39], with a $7 \times 7 \times 7$ k-point mesh for both InGaN and InGaAs. In our calculations, we employed the experimental lattice parameter from [40] and [41] for the binary compounds, and we applied a linear interpolation to find the lattice parameter of the alloy—as suggested by Vurgaftman *et al* [40, 41].

To provide a systematic treatment of our alloys, we employed the GQCA method, which has proved to be a very simple and reliable method to simulate alloys [2, 39, 42–46]. A good description of the method can be found elsewhere [39, 42, 43]. The main idea is to regard the alloy as a large ensemble of clusters containing the same number of atoms, and to study each cluster separately. In principle, the larger the cluster, the more accurate is the description of the alloy, but also the heavier the computational cost, and hence a compromise between accuracy and computational resources is always mandatory. In our case, the alloying process takes place only on the cation sublattice (among In and Ga atoms). Figure 1 shows two different supercells employed in this work. All the possible configurations are studied, which means that, taking symmetry into account, five (16) different clusters are expected considering the cell with eight atoms (16 atoms).

For a given composition x of the alloy, each cluster j with a certain number of In and Ga atoms is realized with a certain probability $p_j(x)$, at a determined temperature (considered here as the usual growth temperature, $T = 900$ K for InGaN and $T = 1000$ K for InGaAs). The configurationally averaged BG, $E_g(x)$, results from a sum over all individual cluster BGs $E_{g,j}$, weighted by the probability $p_j(x)$ of occurrence of each cluster:

$$E_g(x) = \sum_j p_j(x) E_{g,j}. \tag{9}$$

The BG of each cluster, $E_{g,j}$, was calculated within the methods LDA-1/2, HSE03, HSE06 and G_0W_0. The CUT parameters (necessary for LDA-1/2 calculations) for In d, Ga d, As p and N p were extracted from [20]. For each ion, an initial DFT calculation was performed, allowing the ions to relax until an equilibrium position was reached—the maximum accepted force (for any ion) was 1 meV $Å^{-1}$. After this DFT step, ions were kept fixed, and then the BG was calculated using the methods mentioned before. For G_0W_0 calculations, we increased the number of bands to 300. The starting point for G_0W_0 was PBE, and, for InGaN, also HSE03, since PBE proved to be a bad starting point for G_0W_0.

The calculations detailed in the above paragraph were performed with an eight-atom supercell. In a second moment, we increased the size of our supercell to 16 atoms. However, as the HSE03, HSE06 and G_0W_0 calculations turned out to be heavy, we decided to perform only LDA and LDA-1/2 calculations. The procedure considering the larger supercell was analogous to that with the eight-atom supercell. Despite being not strictly necessary, we decided to maintain the employed $7 \times 7 \times 7$ k-point mesh for InGaN supercells, and for InGaAs supercells we even increased this number to $9 \times 9 \times 9$. This can be easily done with LDA and LDA-1/2 methods, once the required computational resources (time and memory) are low.

3. Results and discussion

3.1. Preliminary results: the binaries

Before proceeding to the InGaAs and InGaN alloys, in order to provide an initial overview of our results, the BGs for the binary compounds are shown in table 1. No spin–orbit coupling was taken into account in our calculations, but, aiming to better compare with the experimental measurements, for the arsenides—where the spin–orbit coupling may play an important role—the experimental $\Delta_{SO}/3$ was subtracted from our BGs.

For comparison, table 1 also shows BGs extracted from the literature. One observes that, in general, the present results for BGs exhibit a good agreement with the ones obtained by other groups employing the same methods as here. Concerning the experimental BGs, as expected, LDA severely underestimates the BGs in all four cases, and, concerning InAs and InN, a semimetallic behavior is even predicted, instead of a semiconductor one[3]: LDA predicts too shallow d electrons, and the p–d repulsion pushes the top of the valence band states (which have p character) to higher energies, yielding a greater BG

[3] Actually, the negative BG reported here refers to the inverted ordering of Γ_{1c} and Γ_{15v} states. For instance, the 'true' calculated BG would be zero, as the Fermi level, in LDA calculations, crosses the valence band eigenvalues, and therefore the difference between the unoccupied eigenstates and the occupied ones is zero. However, mentioning this negative BG is a common practice in the literature. For further information, we refer to [47–56].

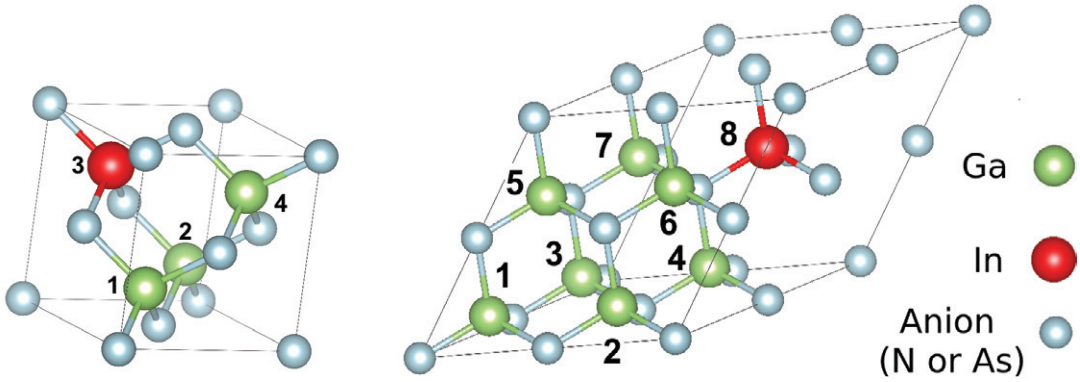

Figure 1. Example of an eight-atom supercell (left) and a 16-atom supercell (right) employed. Green, red and blue spheres represent, respectively, Ga, In and As (or N, accordingly to the studied alloy) atoms. By placing In and Ga atoms in the positions listed as 1, 2, 3 and 4 (or 1, 2, … , 8, for the larger supercell), we are able to reach all the different configurations. Taking the symmetry into account, there exist only five energetically different configurations for the eight-atom supercell (see table 2) and 16 energetically different configurations for the 16-atom supercell (see table 5).

Table 1. Comparison between the experimental and the theoretical BGs (in eV) of the binary compounds GaAs, InAs, GaN and InN.

	Exp.	LDA	LDA-1/2	HSE03	HSE06	G_0W_0	G_0W_0(2)
GaAs	1.519[a]	**0.27** 0.22[c]	**1.34** 1.41[u],1.42[v]	**1.19** 1.08[q], 1.12[i]	**1.35** 1.18[o], 1.33[t]	**1.36** 1.20[c], 1.30[s]	
InAs	0.417[a]	**−0.53** −0.55[c], −0.52[p] −0.46[z], −0.18[w]	**0.34** 0.75[u], 0.42[v]	**0.34** 0.23[q]	**0.39** 0.36[o], 0.42[t]	**0.25** 0.19[c], 0.35[w] 0.42[z]	
GaN	3.299[b]	**1.78** 1.64[h], 1.67[m] 1.81[c], 1.88[f]	**3.43** 3.514[x]	**2.80** 2.65[i], 2.70[m]	**3.03** 2.92[m], 3.02[l]	**2.86** 2.76[f], 2.80[s] 2.88[d], 2.95[m] 3.03[c], 3.1[e]	**3.37** 3.16–3.61[j] 3.29[i], 3.45[m]
InN	0.78[b]	**−0.40** −0.40[y], −0.38[i,n] −0.36[g,i,k], −0.26[c]	**1.08** 0.543[x]	**0.35** 0.37[n]	**0.52** 0.57[k]	**−0.08** −0.13[k], 0.00[i,n] 0.01[c]	**0.36** 0.27–0.54[j] 0.46[k], 0.47[i,n]

Note: Whereas standard G_0W_0 was performed on top of PBE (in most of the references we are comparing our results with, G_0W_0 was calculated starting from LDA, rather than PBE—however, the difference is small), G_0W_0(2) was carried out on top of HSE03. Whereas we exhibit our computed BGs highlighted in bold with neither super- nor subscripts, numbers appearing with superscripts were reported in the literature. The experimental BGs were extracted from [a] [40], [b] [41]. The experimental spin–orbit coupling parameters, Δ_{SO}, are 0.341 and 0.39 eV for GaAs and InAs, respectively [40]. Other theoretical results were extracted from [c] [47], [d] [65], [e] [66], [f] [67], [g] [52], [h] [68], [i] [64], [j] [53] (for this reference, G_0W_0(2) was performed on top of HSE06), [k] [69] (for this reference, G_0W_0(2) was performed on top of HSE06), [l] [70], [m] [6], [n] [10], [o] [71], [p] [48], [q] [72], [r] [73], [s] [74], [t] [75], [u] [20], [v] [76], [w] [50] (for the safe of a better comparison, we subtracted $\Delta_{SO}/3$ from their results to show here), [x] [77], [y] [78], [z] [49].

underestimation than observed for LDA-BGs in other compounds [52]. For all the binaries, LDA-1/2 does improve the BG predictions, and the discrepancy is strongly reduced; furthermore, LDA-1/2 brings the predicted BGs near to experimental ones. From this, we may conclude that, for these materials, LDA-1/2 introduces a correction to the KS potential that results in improving the quality of the eigenvalues: they can now get closer to the experimental BGs. The same tendency is observed for LDA-1/2 applied to other materials [20–22]. Also in the literature, one can find other corrections to the KS potential that increase the agreement between experimental and calculated BGs. Concerning the adjustment to the Tran–Blaha modified Becke–Johnson potential proposed by Hong Jiang to avoid self-consistency [57], he found BGs for InN (1.01 eV, for wurtzite), GaN (3.05 eV), InAs (0.46 eV) and GaAs (1.44 eV) similar to our LDA-1/2 results. For the nitrides, the BGs calculated within the hybrid functional PBE0 also agree well with our LDA-1/2 results: Wu *et al* found 1.09 eV for InN and 3.52 eV for GaN [58]; something similar also happens with the self-interaction corrected method (Sökeland *et al* obtained 1.3 eV for the BG of InN, and 3.5 eV for GaN [59]), and also for the optimized effective potential (OEP) with the exact exchange (EXX) functional (Betzinger *et al* obtained 0.98 eV for InN and 3.11 eV for GaN [60]; Klimeš *et al* got 3.12 eV for GaN with EXX-OEP as well [61]). On the other hand, for InAs and GaAs, BGs calculated within PBE0 and EXX-OEP methods tend to be higher than those found within the LDA-1/2 method: PBE0 BGs are 1.0 eV for InAs and 1.9 eV for GaAs [62], while EXX-OEP predicts GaAs BG to be 1.72–1.77 eV [61, 63]—however, in these cases, employing the LDA-1/2 method results in better agreement with the experimental BGs, as can be verified in table 1.

The hybrid functionals also exhibit a nice performance for the BGs here calculated: while HSE03 greatly diminishes the

Table 2. List of energetically different clusters considering an eight-atom supercell (four cations and four anions) and their respective BGs as calculated by using LDA, LDA-1/2, HSE03, HSE06 and G_0W_0.

				Gap-InGaAs (eV)					Gap-InGaN (eV)					
Cluster	n_{In}	Position	Deg.	LDA	LDA-1/2	HSE03	HSE06	G_0W_0	LDA	LDA-1/2	HSE03	HSE06	G_0W_0	G_0W_0 (2)
0	0	—	1	0.38	1.46	1.30	1.47	1.47	1.78	3.43	2.80	3.03	2.86	3.37
1	1	1	4	0.05	1.10	0.90	1.05	1.02	1.04	2.59	1.96	2.18	1.95	2.42
2	2	1, 2	6	−0.03	0.82	0.64	0.36	1.89	0.79	0.84	1.22	1.42	1.04	1.39
3	3	1, 2, 3	4	−0.27	0.65	0.52	0.67	0.55	0.01	1.47	0.80	0.98	0.48	1.01
4	4	1, 2, 3, 4	1	−0.40	0.47	0.38	0.52	0.38	−0.40	1.08	0.35	0.52	−0.08	0.36

Note: The classes of clusters are labeled according to the number of indium atoms (n_{In}) present in the supercell. 'Deg.' denotes the degeneracy of each class, i.e. the number of different configurations which have the same energy (due to symmetry equivalence). Indium atoms are settled following the numbers of figure 1. G_0W_0(2) stands for G_0W_0 applied on top of HSE03.

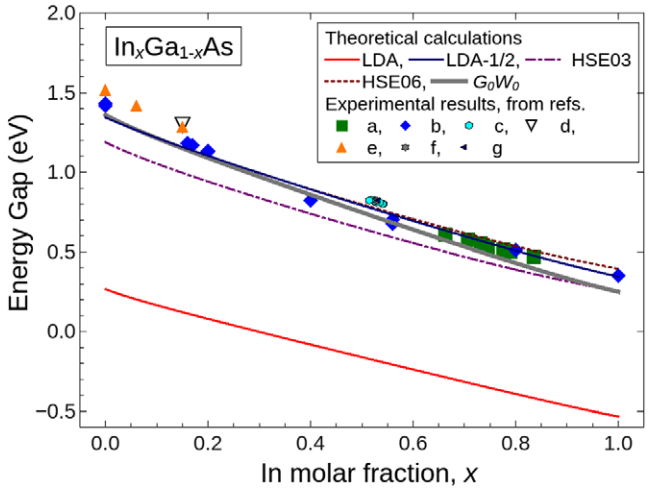

Figure 2. BG of InGaAs alloy: lines are the results of calculations performed in this work, and symbols are experimental results extracted from the literature: a, [79]; b, [80]; c, [81]; d, [82]; e, [83]; f, [84]; g, [85].

BG underestimation observed in LDA, HSE06 achieves a step forward in accuracy, getting closer to the measured BGs.

Finally, QP inclusions within the G_0W_0 approximation have indeed improved BG predictions in comparison with LDA. Concerning InAs and, even more, InN, DFT eigenvalues turned out to be bad starting points for the G_0W_0 calculations: the wrong sequencing of KS eigenvalues arising in the LDA (or GGA) framework may lead to a failure of G_0W_0, since the perturbative G_0W_0 requires a correct ordering of single particle eigenvalues [64]. For InAs, surprisingly, this problem was overcome, but InN required a generalized KS as starting point (HSE03). HSE03 also proved to be a better starting point for G_0W_0 in predicting the BG of GaN.

3.2. Alloys

A common feature of several opto-electronic devices is the use of pseudoternary alloys as InGaN and InGaAs. Alloying among the group III nitrides and arsenides allows us, in principle, to engineer the BG between the two extreme binary values. In table 2 is shown the calculated BG, detailed for the five clusters. We see that the addition of In to the cluster reduces the BG, and the reduction is not directly proportional to the amount of In added: in fact, we cannot encounter a constant relation of shrinkage per percentage of In in the alloy—this fact leads to a non-linear BG curve, as we observe later.

By making use of these BGs, it is straightforward to calculate the BG of the alloys as a continuous function of x. It is worth mentioning that the BGs that appear in table 2 have no spin–orbit effect. This effect may be neglected for the InGaN alloy, but not for the InGaAs. In the latter, $\Delta_{SO}(x)/3$ was subtracted from our results to better compare with the experimental data. The spin–orbit coupling, for InGaAs alloy, as a function of composition, is reported to be [40]

$$\Delta_{SO}(x) = 0.341(1-x) + 0.39x - 0.15x(1-x). \quad (10)$$

The calculated InGaAs BG is shown in figure 2, where experimental data are depicted as symbols. The LDA curve lies well below the experimental points, as expected. HSE03 highly improves this scenario, and diminishes the underestimation of the BG, reaching an error of roughly 0.2 eV. HSE06 performs quite well, competing with G_0W_0 in accuracy. LDA-1/2 results also show a good agreement with experimental data, and, at first sight, one can observe only a slight difference between the results from LDA-1/2, HSE06 and G_0W_0, and it is difficult to decide which of them performs better.

However, by no means are we able to say that any two curves simply differ by a rigid shift, or by applying the 'scissors operator'. This becomes clear when one describes the BG of the alloy by the expression

$$E_g(In_xGa_{1-x}Y) = xE_g(InY) + (1-x)E_g(GaY) - bx(1-x) \quad (11)$$

where Y could stand for As or N, and b is the so-called bowing parameter (and can be fitted to the theoretical curves). The bowing appears in table 3, and we see that each bowing parameter is different from the others, the exception being those obtained by HSE03 and HSE06. We avoid here more comments on the bowing, the reason being that a further section is devoted to this.

The BG of InGaN is depicted in figure 3. For this alloy, considering the difficulties concerning the growth, the experimental points are much more disperse than those of InGaAs alloy. Regarding the In-rich region, measured BGs, taken from

Table 3. Bowing parameters in electron volts.

		LDA	LDA-1/2	HSE03	HSE06	G_0W_0	G_0W_0(2)	Exp.
InGaAs	cel08	0.13	0.22	0.32	0.32	0.25	—	0.477[a]
	cel16	0.22	0.46	—	—	—	—	
InGaN	cel08	0.64	0.80	0.71	0.71	0.69	0.75	1.4[b]
	cel16	1.1	1.3	—	—	—	—	

Note: The experimental results come from [a] [40] and [b] [41].

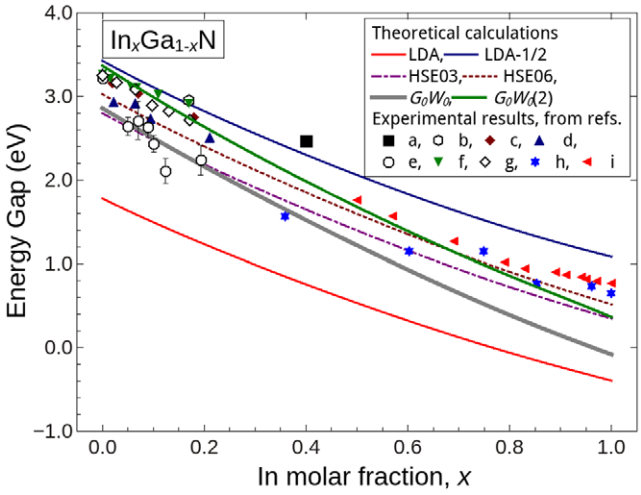

Figure 3. BG of zincblende InGaN alloy as a function of In composition: lines are the results of calculations performed in this work, and symbols are experimental results extracted from the literature: a, [86]; b, [87]; c, [88]; d, [89]; e, [90]; f, [91]; g, [92]; h, [93]; i, [94].

[93] and [94], were only found for wurtzite alloys (which have a BG slightly higher than the zincblende phase). Even concerning the wurtzite phases (which are more stable than their zincblende counterparts), many issues can occur during the growth of InGaN, such as phase separation, regions of pure InN and formation of In metal nanoparticles [95]. These difficulties make the growth of high-quality InGaN samples (and the subsequent BG determination) a very complicated task. Even so, we prefer to introduce this experimental set of data (for wurtzite alloys, grown under these difficulties), aiming to have at least a general overview of whether the methods employed here can reproduce the experimental BGs.

We observe that LDA underestimates the BG, and this is to a great extent remedied by HSE03. HSE06 outperforms HSE03, and fits the data better. The G_0W_0 method performed on top of PBE shows nice agreement (with experimental points) in the Ga-rich region, but, as the In composition increases, the accuracy is reduced, mainly due to the problems arising from the InN BG predicted by PBE. LDA-1/2 turned out to perform a good fit to the experimental points in the Ga-rich range of compositions. From this figure, we can also conclude that the best qualitative agreement with the experimental data is reached by HSE06 and G_0W_0 performed on top of HSE03, although this is not a rigorous conclusion.

Up to now, we have compared the BG prediction for InGaAs and InGaN, considering several calculation methods, and our comparison was driven basically by qualitative judgments. A step further is to quantify the agreement between each approach and the experimental data, since this would help to decide on the most accurate method—it would also be interesting to compare this overall accuracy with the computational effort demanded, so that one could fairly decide on one approach, knowing 'how much it would cost', in terms of computation—and this is what we do in the following section.

3.3. Accuracy and computational resources

To provide a quantitative measurement of how the BG predicted by each method fits the experimental points, we considered the root mean square error (ER) defined by

$$\mathrm{ER} = \sqrt{\frac{1}{N}\sum_i (\text{Predicted Gap} - \text{Measured Gap})_i^2}, \quad (12)$$

where i sweeps all the experimental points shown in figure 2 or figure 3.

The errors ER incurred by each calculation approach are given in table 4. For instance, considering this measure of error, the InGaAs BG is best obtained by the hybrid functional HSE06, whereas its hybrid counterpart, HSE03, brought about the largest error. LDA-1/2 and G_0W_0 turned out to have, basically, the same accuracy. Turning our attention to InGaN, we notice that, once more, HSE06 was found to have the highest degree of accuracy—in this case, G_0W_0 performed on top of HSE03 provided BGs basically as accurate as those of HSE06. LDA-1/2 and HSE03 had essentially the same accuracy, and G_0W_0 performed on top of PBE was the least accurate; this is not surprising, considering the points raised about InAs in section 3.1.

It is interesting to note that the error ER more than doubles when we move from InGaAs to InGaN. We attribute this fact to two sources: (a) the higher InGaN BG, which is almost double the InGaAs BG (in fact, if we suppose that the error is proportional to the BG, an increase in the error is expected when the BG increases), and (b) the more disperse experimental data available for InGaN alloy (as a matter of fact, this implies that each single experimental point is less reliable when we are dealing with InGaN than when we are dealing with InGaAs).

However, solely a raw comparison of accuracy, as done before, is not totally fair: one approach, could, for example, require a much larger computational effort to reach that level of accuracy, and when deciding on which approach should be employed one should be aware of the computational price beforehand. Therefore, we also compare the computational resources (average time, T, and memory, M) demanded by each

Table 4. Required computational resources and accuracy (measured by the root mean square error, ER, in eV) of each approach.

	InGaAs					InGaN					
	LDA-1/2		HSE03	HSE06	G_0W_0	LDA-1/2		HSE03	HSE06	G_0W_0	G_0W_0(2)
	8 atoms	16 atoms	8atoms			8 atoms	16 atoms	8 atoms			
T	0.005	0.03	4.7	3.0	18.0	0.01	0.02	4.6	3.7	13.5	15.8
M	0.7	0.8	1.4	1.4	32.0	1.1	2.3	1.2	1.2	30.2	30.2
ER	0.10	0.09	0.19	0.06	0.09	0.39	0.35	0.40	0.25	0.52	0.28

Note: The computational time (T, given in hours) and the memory (M, given in GB) were averaged among all the clusters employed in GQCA.

Table 5. Energy gap of energetically different clusters, with their respective degeneracies (Deg.), considering a 16-atom supercell: the clusters are labeled according to the number of indium atoms n_{In} contained in each one, and the positions of such indium atoms follow the numbers shown in figure 1.

				Gap-InGaAs (eV)		Gap-InGaN (eV)	
Cluster	n_{In}	Position	Deg.	LDA	LDA-1/2	LDA	LDA-1/2
0	0	—	1	0.38	1.46	1.78	3.43
1	1	1	8	0.15	1.21	1.33	2.94
2	2	1,2	24	0.05	0.97	0.87	2.46
3	2	4,5	4	0.05	1.09	1.04	2.59
4	3	1,2,3	32	−0.08	0.81	0.59	2.14
5	3	1,4,5	24	−0.12	0.90	0.64	2.19
6	4	1,2,3,4	8	−0.10	0.66	0.29	1.82
7	4	1,2,3,5	8	−0.33	0.68	0.33	1.85
8	4	1,2,4,5	48	0.02	0.75	0.36	1.88
9	4	2,4,5,7	6	−0.19	0.81	0.36	1.89
10	5	1,2,3,4,5	32	−0.41	0.60	0.10	1.61
11	5	1,2,3,6,7	24	−0.29	0.69	0.15	1.65
12	6	1,2,3,4,5,6	24	0.04	0.54	0.05	1.39
13	6	1,2,3,6,7,8	4	−0.27	0.65	0.01	1.47
14	7	1,2,3,4,5,6,7	8	−0.40	0.52	−0.24	1.24
15	8	1,2,3,4,5,6,7,8	1	−0.40	0.47	−0.40	1.08

approach. All of our calculations were run in parallel on two Intel CPUs, each one containing 10 cores, operating at 3.0 GHz. The results for T and M appear in table 4. When it comes to the memory, basically, all the methods require much the same amount, G_0W_0 being an exception, for which an increase of one order of magnitude was observed. However, regarding the computational time, the scenario is quite different: LDA-1/2 basically benefits from its DFT-like formulation, and, hence, requires much less time. It is worth mentioning that the hybrid functionals demand on average a calculation time two orders of magnitude longer than the LDA-1/2 one; referring to G_0W_0, this number increases to three orders of magnitude.

A final conclusion is that, considering the alloys studied here, and the *ab initio* approaches employed in this work, the best compromise between accuracy and computational effort has been achieved by the LDA-1/2 method, which succeeded in giving basically the same accuracy as G_0W_0, but at the computational price of a standard DFT calculation. This conclusion goes in the same direction as those of [76] and [96].

3.4. Increasing the supercell size to 16 atoms

We have devoted the last section to discussing the accuracy of our *ab initio* approaches. However, the accuracy of simulating an alloy does not depend only on the accuracy of describing the (generalized) KS eigenvalues (or the QP eigenvalues); it also hinges upon the quality of the clusters which comprise the alloy. On one hand, for the sake of accuracy, increasing the supercell size leads to an improvement of the description of the cluster expansion which describes the alloy. Comparing to a smaller supercell, a larger set of configurations enabled by the larger supercell allows us to better 'sample' not only the smaller (and the higher) concentrations, but also less symmetric configurations with an intermediate composition. On the other hand, for the sake of computational involvement, a minimal sized supercell is mandatory, as larger supercells are computationally heavier, not only considering the memory and the time required by a single calculation, but also considering that more configurations will appear, and may demand more calculations than the smaller supercell. The computational cost may grow in a such a way that it may become prohibitive for the heavier methods (such as G_0W_0 and hybrid functionals).

Here, we address the effect of doubling the size of our supercell. Considering the increase in the computational effort, we restrict our study with this larger supercell to the LDA and the LDA-1/2 method.

In table 5, we detail the BG of each cluster which appears in the new expansion. From these results, the BG calculation

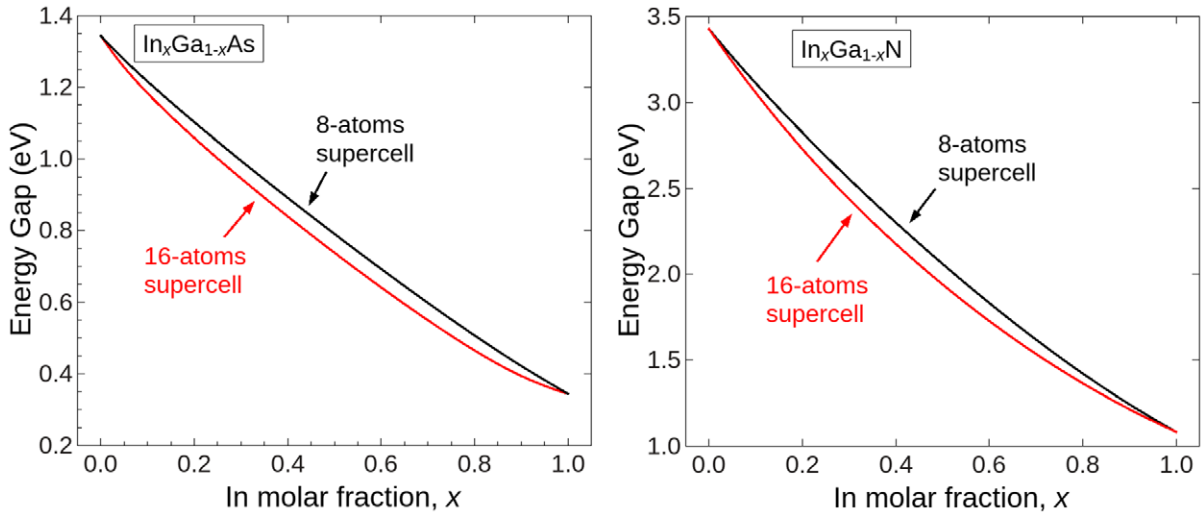

Figure 4. Effect of increasing the supercell size (from 8 atoms to 16 atoms) on the BGs: InGaAs on the left and InGaN on the right.

of the alloys follows naturally, and it is shown in figure 4, where we contrast BGs computed within an eight-atom supercell and a 16-atom supercell.

The differences between the two curves appear to be minimal: in fact, the largest difference in BG predicted with an expansion with the eight-atom supercell and with the 16-atom supercell is 0.053 eV for InGaAs, and 0.122 eV for InGaN. From this point of view, it does not seem worthwhile to increase the size of our supercell. Even so, the curvature is highly affected by this modification.

This means that the BG bowing parameter is more sensitive to the increase in the supercell (regarding an increase from eight atoms to 16 atoms). This is reported in table 3. We note that the bowing is not yet converged[4] with the eight-atom supercell: in fact, almost a doubling in the bowing value is observed when the size of the supercell is doubled. On the other hand, with this more converged 16-atom supercell, the bowing parameter predicted by the LDA-1/2 method shows very good agreement with the experimental one, for both InGaAs and InGaN alloys. Also, for InGaN, the LDA bowing is surprisingly good in comparison with the experimental one, which does not happen for InGaAs.

The bowing parameters predicted by HSE03, HSE06 and G_0W_0 do not reach a good accuracy, in principle, due to the non-converged results for the eight-atom supercell. However, we can introduce a correction factor, regarding the increase observed in the LDA-1/2 bowing. If we apply this proportional factor, the bowing predicted for InGaAs by HSE03, HSE06 and G_0W_0 changes, respectively, to 0.67, 0.67 and 0.52 eV, which in turn exhibits a nice agreement with the reported bowing (0.477 eV). Concerning InGaN, the corrected bowing is 1.15, 1.15, 1.12 and 1.22 eV, respectively, for HSE03, HSE06, G_0W_0 (on top of GGA) and G_0W_0 (on top of HSE03)—these results are also in good accordance with the reported one (1.4 eV).

[4] Here, as we did not make further calculations for even larger cells, by 'converged result' we mean 'in better agreement with the measured one'.

A final comment on the increase of the supercell is that it provided an improvement in the overall accuracy (the ER slightly decreased for InGaAs BG, and presented a greater decrease for InGaN BG), without an alarming increase in the computational cost: time and memory turned out to increase, but they still remain treatable in the LDA-1/2 framework.

4. Conclusions

In this article, we compared the performance (in terms of accuracy, and also computational resources, such as time and memory, required for calculations) of four *ab initio* approaches that can be used to obtain BGs: LDA-1/2, HSE03, HSE06 and G_0W_0. With these methods, we obtained the BG of zincblende InGaAs and InGaAs alloys, chosen as benchmarks, employing also a rigorous statistical approach (the GQCA method, in an eight-atom supercell). For these alloys, we observed that the HSE06 method provided the most accurate BGs (in comparison with experiments). However, when it came to the best compromise between accuracy and computational resources, the LDA-1/2 method was shown to outperform the others, reaching an accuracy comparable with G_0W_0, but at the same computational cost of a standard DFT calculation. Regarding the low computational price demanded by LDA-1/2, we increased the supercell size to 16 atoms, and verified the effect on the BG and the bowing parameter. The BG showed minor changes, whereas the bowing unveiled its convergence only for the larger supercell.

Acknowledgments

The authors are grateful for support received from Alexander von Humboldt-Stiftung, Coordenação de Aperfeiçoamento de Pessoal de Nível Superior (CAPES), Conselho Nacional de Desenvolvimento Científico e Tecnológico (CNPq), and from grant 2012/50738-3, São Paulo Research Foundation (FAPESP).

References

[1] Adachi S 2005 *Properties of Group-IV, III–V and II–VI Semiconductors* (New York: Wiley)
[2] Pelá R R, Caetano C, Marques M, Ferreira L G, Furthmüller J and Teles L K 2011 *Appl. Phys. Lett.* **98** 151907
[3] van Schilfgaarde M, Sher A and Chen A B 1997 *J. Cryst. Growth* **178** 8
[4] Hedin L 1965 *Phys. Rev.* **139** A796
[5] Walsh A, Catlow C R A and Sokol A A (ed) 2013 *Computational Approaches to Energy Materials* (New York: Wiley)
[6] Mietze C, Landmann M, Rauls E, Machhadani H, Sakr S, Tchernycheva M, Julien F H, Schmidt W G, Lischka K and As D J 2011 *Phys. Rev.* B **83** 195301
[7] Landmann M, Rauls E, Schmidt W G, Röppischer M, Cobet C, Esser N, Schupp T, As D J, Feneberg M and Goldhahn R 2013 *Phys. Rev.* B **87** 195210
[8] van Schilfgaarde M, Kotani T and Faleev S 2006 *Phys. Rev. Lett.* **96** 226402
[9] Rödl C, Fuchs F, Furthmüller J and Bechstedt F 2009 *Phys. Rev.* B **79** 235114
[10] Bechstedt F, Fuchs F and Kresse G 2009 *Phys. Status Solidi b* **246** 1877–92
[11] Heyd J, Scuseria G E and Ernzerhof M 2003 *J. Chem. Phys.* **118** 8207
[12] Perdew J P, Burke K and Ernzerhof M 1996 *Phys. Rev. Lett.* **77** 3865–8
[13] Heyd J, Peralta J E, Scuseria G E and Martin R L 2005 *J. Chem. Phys.* **123** 174101
[14] Paier J, Marsman M, Hummer K, Kresse G, Gerber C and Ángyán J G 2006 *J. Chem. Phys.* **124** 154709
[15] Marsman M, Paier J, Stroppa A and Kresse G 2008 *J. Phys.: Condens. Matter* **20** 064201
[16] Nicklas W and Wilkins J W 2010 *Appl. Phys. Lett.* **97** 091902
[17] Komsa H P, Broqvist P and Pasquarello A 2010 *Phys. Rev.* B **81** 205118
[18] Chen W, Tegenkamp C, Pfnür H and Bredow T 2010 *Phys. Rev.* B **82** 104106
[19] von Bardeleben H J *et al* 2012 *Phys. Rev. Lett.* **109** 206402
[20] Ferreira L G, Marques M and Teles L K 2008 *Phys. Rev.* B **78** 125116
[21] Ferreira L G, Marques M and Teles L K 2011 *AIP Adv.* **1** 032119
[22] Ferreira L G, Pelá R R, Teles L K, Marques M, Ribeiro M Jr and Furthmüller J 2013 *AIP Conf. Proc.* **27** 1566
[23] Ullrich C A 2012 *Time-Dependent Density-Functional Theory, Concepts and Applications* (New York: Oxford University Press)
[24] Pelá R R, Marques M, Ferreira L G, Furthmüller J and Teles L K 2012 *Appl. Phys. Lett.* **100** 202408
[25] Santos J P T, Marques M, Ferreira L G, Pelá R R and Teles L K 2012 *Appl. Phys. Lett.* **101** 112403
[26] Ribeiro M Jr, Ferreira L, Fonseca L and Ramprasad R 2012 *Mater. Sci. Eng.* B **177** 1460–4
[27] Ribeiro M Jr, Fonseca L R C, Sadowski T and Ramprasad R 2012 *J. Appl. Phys.* **111** 073708
[28] Filho O P S, Ribeiro M Jr, Pelá R R, Teles L K, Ferreira L G and Marques M 2013 *J. Appl. Phys.* **114** 033709
[29] Matusalem F, Ribeiro M Jr, Marques M, Pelá R R, Ferreira L G and Teles L K 2013 *Phys. Rev.* B **88** 224102
[30] Matusalem F, Pelá R R, Marques M and Teles L K 2014 *Phys. Rev.* B **90** 224102
[31] Slater J C and Johnson K H 1972 *Phys. Rev.* B **5** 844
[32] Janak J F 1978 *Phys. Rev.* B **18** 7165
[33] Leite J R and Ferreira L G 1971 *Phys. Rev.* A **3** 1224–30
[34] Lam Y, Loehr J and Singh J 1992 *IEEE J. Quantum Electron.* **28** 1248–60
[35] Capasso F, Faist J, Sirtori C and Cho A Y 1997 *Solid State Commun.* **102** 231
[36] Pelá R R, Teles L K, Marques M and Martini S 2013 *J. Appl. Phys.* **113** 033515
[37] Kresse G and Hafner J 1993 *Phys. Rev.* B **47** R558
[38] Kresse G and Furthmüller J 1996 *Comput. Mater. Sci.* **6** 15
[39] Teles L K, Furthmüller J, Scolfaro L M R, Leite J R and Bechstedt F 2000 *Phys. Rev.* B **62** 2475
[40] Vurgaftman I, Meyer J R and Ram-Mohan L R 2001 *J. Appl. Phys.* **89** 5815
[41] Vurgaftman I and Meyer J R 2003 *J. Appl. Phys.* **94** 3675
[42] Chen A B and Sher A 1995 *Semiconductor Alloys* (New York: Plenum)
[43] Caetano C, Teles L K, Marques M, Dal Pino A and Ferreira L G 2006 *Phys. Rev.* B **74** 045215
[44] de Carvalho L C, Schleife A, Furthmüller J and Bechstedt F 2012 *Phys. Rev.* B **85** 115121
[45] Santos J P T, Marques M, Teles L K and Ferreira L G 2010 *Phys. Rev.* B **81** 115209
[46] Teles L K, Scolfaro L M R, Leite J R, Furthmüller J and Bechstedt F 2002 *J. Appl. Phys.* **92** 7109–13
[47] Kotani T and van Schilfgaarde M 2002 *Solid State Commun.* **121** 461
[48] Massidda S, Continenza A, Freeman A J, de Pascale T M, Meloni F and Serra M 1990 *Phys. Rev.* B **41** 12079–85
[49] Malone B D and Cohen M L 2013 *J. Phys.: Condens. Matter* **25** 105503
[50] Lebègue S, Arnaud B, Alouani M and Bloechl P E 2003 *Phys. Rev.* B **67** 155208
[51] Zanolli Z, Fuchs F, Furthmüller J, von Barth U and Bechstedt F 2007 *Phys. Rev.* B **75** 245121
[52] Furthmüller J, Hahn P H, Fuchs F and Bechstedt F 2005 *Phys. Rev.* B **72** 205106
[53] de Carvalho L C, Schleife A and Bechstedt F 2011 *Phys. Rev.* B **84** 195105
[54] Bechstedt F and Furthmüller J 2002 *J. Cryst. Growth* **246** 315–9 (Proc. Int. Workshop on Bulk Nitride Semiconductors)
[55] Bechstedt F, Furthmüller J, Ferhat M, Teles L K, Scolfaro L M R, Leite J R, Davydov V Y, Ambacher O and Goldhahn R 2003 *Phys. Status Solidi a* **195** 628–33
[56] Stampfl C, Van de Walle C G, Vogel D, Krüger P and Pollmann J 2000 *Phys. Rev.* B **61** R7846
[57] Jiang H 2013 *J. Chem. Phys.* **138** 134115
[58] Wu X, Walter E J, Rappe A M, Car R and Selloni A 2009 *Phys. Rev.* B **80** 115201
[59] Sökeland F, Rohlfing M, Krüger P and Pollmann J 2003 *Phys. Rev.* B **68** 075203
[60] Betzinger M, Friedrich C, Görling A and Blügel S 2012 *Phys. Rev.* B **85** 245124
[61] Klimeš J and Kresse G 2014 *J. Chem. Phys.* **140** 054516
[62] Tomić S and Harrison N M 2010 *AIP Conf. Proc.* **1199** 65–6
[63] Betzinger M, Friedrich C, Blügel S and Görling A 2011 *Phys. Rev.* B **83** 045105
[64] Fuchs F, Furthmüller J, Bechstedt F, Shishkin M and Kresse G 2007 *Phys. Rev.* B **76** 115109
[65] Rohlfing M, Krüger P and Pollmann J 1998 *Phys. Rev.* B **57** 6485–92
[66] Rubio A, Corkill J L, Cohen M L, Shirley E L and Louie S G 1993 *Phys. Rev.* B **48** 11810–6
[67] Palummo M, Reining L, Godby R W, Bertoni C M and Börnsen N 1994 *Europhys. Lett.* **26** 607
[68] Rinke P, Winkelnkemper M, Qteish A, Bimberg D, Neugebauer J and Scheffler M 2008 *Phys. Rev.* B **77** 075202
[69] Duan Y, Qin L, Shi L, Tang G and Shi H 2014 *J. Phys.: Condens. Matter* **26** 025501
[70] Qin L, Duan Y, Shi H, Shi L and Tang G 2013 *J. Phys.: Condens. Matter* **25** 045801

[71] Lucero M J, Henderson T M and Scuseria G E 2012 *J. Phys.: Condens. Matter* **24** 145504
[72] Peralta J E, Heyd J, Scuseria G E and Martin R L 2006 *Phys. Rev.* B **74** 073101
[73] Kim Y S, Hummer K and Kresse G 2009 *Phys. Rev.* B **80** 035203
[74] Shishkin M and Kresse G 2007 *Phys. Rev.* B **75** 235102
[75] Kim Y S, Marsman M, Kresse G, Tran F and Blaha P 2010 *Phys. Rev.* B **82** 205212
[76] Belabbes A, Panse C, Furthmüller J and Bechstedt F 2012 *Phys. Rev.* B **86** 075208
[77] Belabbes A, de Carvalho L C, Schleife A and Bechstedt F 2011 *Phys. Rev.* B **84** 125108
[78] Stampfl C and Van de Walle C G 1999 *Phys. Rev.* B **59** 5521–35
[79] Kim D S, Forrest S R, Lange M J, Cohen M J, Olsen G H, Menna R J and Paff R J 1996 *J. Appl. Phys.* **80** 6229
[80] Williams E W and Rehn V 1968 *Phys. Rev.* **172** 798
[81] Goetz K H, Bimberg D, Jürgensen H, Selders J, Solomonova A V, Glinskii G F and Razeghi M 1983 *J. Appl. Phys.* **54** 4543
[82] Marzin J Y, Charasse M N and Sermage B 1985 *Phys. Rev.* B **31** 8298
[83] Hang Z, Yan D, Pollak F H, Pettit G D and Woodall J M 1991 *Phys. Rev.* B **44** 10546
[84] Towe E 1982 *J. Appl. Phys.* **53** 5136
[85] Zielinski E, Schweizer H, Streubel K, Eisele H and Weimann G 1986 *J. Appl. Phys.* **59** 2196
[86] Müllhäuser J R, Brandt O, Trampert A, Jenichen B and Ploog K H 1998 *Appl. Phys. Lett.* **73** 1230
[87] Müllhäuser J R, Jenichen B, Wassermeier M, Brandt O and Ploog K H 1997 *Appl. Phys. Lett.* **71** 909
[88] Goldhahn R, Scheiner J, Shokhovets S, Frey T, Köhler U, As D J and Lischka K 2000 *Appl. Phys. Lett.* **76** 291
[89] Chichibu S F *et al* 2001 *Appl. Phys. Lett.* **79** 3600
[90] Kitamura T, Cho S, Ishida Y, Ide T, Shen X Q, Nakanishi H, Chichibu S and Okumura H 2001 *J. Cryst. Growth* **227–8** 471
[91] Brandt O, Mullhauser J, Yang B, Yang H and Ploog K 1998 *Physica* E **2** 532–8
[92] Pacheco-Salazar D G, Leite J R, Cerdeira F, Meneses E A, Li S F, As D J and Lischka K 2006 *Semicond. Sci. Technol.* **21** 846
[93] Davydov V Y *et al* 2002 *Phys. Status Solidi* B **230** R4
[94] Wu J, Walukiewicz W, Yu K M, Arger J W III, Haller E E, Lu H and Schaff W J 2002 *Appl. Phys. Lett.* **80** 4741
[95] Ivanov S V, Shubina T V, Komissarova T A and Jmerik V 2014 *J. Cryst. Growth* **403** 83–9
[96] Belabbes A, Furthmüller J and Bechstedt F 2011 *Phys. Rev.* B **84** 205304